Journal of Photochemistry and Photobiology A: Chemistry 205 (2009) 139–144

Contents lists available at ScienceDirect

Journal of Photochemistry and Photobiology A: Chemistry

journal homepage: www.elsevier.com/locate/jphotochem

Photoinduced intermolecular and intramolecular charge transfer in the mixed coaggregates of pyrazoline and dicyanonaphthalene

Yuanzuo Li [a], Shasha Liu [a], Maodu Chen [a,*], Fengcai Ma [b]

[a] School of Physics and Optoelectronic Technology, and College of Advanced Science and Technology, Dalian University of Technology, Dalian 116024, PR China
[b] Department of Physics, Liaoning University, Shenyang 110036, PR China

ARTICLE INFO

Article history:
Received 24 December 2008
Received in revised form 26 March 2009
Accepted 22 April 2009
Available online 3 May 2009

Keywords:
Charge transfer
Excited state
2D site representation
3D cube representation
Transition dipole moment

ABSTRACT

Photoinduced charge transfer (CT) and excited state properties in the mixed coaggregates of 1,3,5-triphenyl-2-pyrazoline (TPP) and 1,4-dicyanonaphthalene (DCN) are investigated theoretically, using time-dependent density functional theory (TD-DFT) as well as the two-dimensional (2D) site (transition density matrix) and three-dimensional (3D) cube (transition density and charge difference density) representations. The calculated results indicate that a strong absorption band stems from the $S_0 \rightarrow S_4$ transition. There are electron–hole coherences between TPP and DCN monomers, which are shown by 2D site representation. Direct visual evidence revealed by 3D cube representations indicates that photoinduced CT mechanism for the mixed coaggregates of TPP and DCN is the mixture of intermolecular and intramolecular CT in the vertical absorption. Some phenyl group of TPP monomer not only serves as the electronic donor in the intramolecular CT, but also in the intermolecular CT process.

1. Introduction

Photoinduced charge transfer (CT) from donor to acceptor is a primary step in photophysical, photochemical as well as photobiological processes [1–5]. The charge transfer process can be intermolecular CT in which an electron is transferred from electron-donating species (D) to electron-accepting species (A), producing the radical cation of donor and the radical anion of acceptor, or intramolecular CT, involving charge redistribution in the excited molecule which produces a very large excited state dipole moment. Much effort has been invested to understand the fine details of inter- and or intra-molecular CT processes [6–13]. Although a great variety of molecular systems (from directly linked D–A compounds to D–π–A compounds) have been elaborated [6–9], and although the covalently linked and hydrogen-bonded donor–acceptor coaggregates also exhibit excellent CT characteristics [10–13], photoinduced charge transfer for mixed coaggregates with electron-rich and electron-deficient components has been a little attention [14]. The possible mechanism of the reaction has not been investigated so far.

It is well known that photophysical properties of the organic molecules are determined predominantly by the low energy excited states. Knowledge of nature of excited states, and interplay of inter- and intra-molecular mechanism in the CT process, are becoming very important to develop the novel optoelectronic device. For mixed coaggregates, bimolecular interactions between an excited donor and a ground-state acceptor sometimes lead to the complex photophysical and or photochemical phenomena [15–19]. For example, those interactions give rise to the exciplex [17] and affect the emission spectra by developing a new structureless band at a longer wavelength region [18,19]. There are two possible pathways of electron transition to form exciplex: the first one is direct electronic transition from the HOMO of one entity to the LUMO of another entity; the other one is via the transition of one electron from the LUMO of one entity to the LUMO of another. The ground and excited ICT state of weak complex can be described in terms of wave function [20]:

$$\psi_g = a\psi_0(\mathrm{D,A}) + b\psi_1(\mathrm{D^+A^-}) \quad (1)$$

$$\psi_E = a^*\psi_1(\mathrm{D^+A^-}) - b^*\psi_0(\mathrm{D,A}) \quad (2)$$

where a and b describe the contribution of each structure to wave function. $\psi_0(\mathrm{D,A})$ is the configuration for the normal, weakly bound complex, and $\psi_1(\mathrm{D^+A^-})$ is the CT configuration. In Eq. (1), $\psi_0(\mathrm{D,A})$ make great contribution to the ground state because of very small resonance energy in the ionic structure $\psi_1(\mathrm{D^+A^-})$. For excited state, the ionic form becomes the predominant ($|a| \geq |b|$) because an electron is transferred from the donor to the acceptor. In this CT process, excited molecule should experience geometry modification in some segments of molecules (where the arrangement of electron–hole pairs occurs), exhibiting an obvious change of transition dipole moment (which can be approximated as $\mu_{eg} \approx a^* b\mu_{11} + aa^*\mu_{01}$ [21],

* Corresponding author. Tel.: +86 411 84706101 604.
E-mail address: mdchen@dlut.edu.cn (M. Chen).

1010-6030/$ – see front matter © 2009 Elsevier B.V. All rights reserved.
doi:10.1016/j.jphotochem.2009.04.019

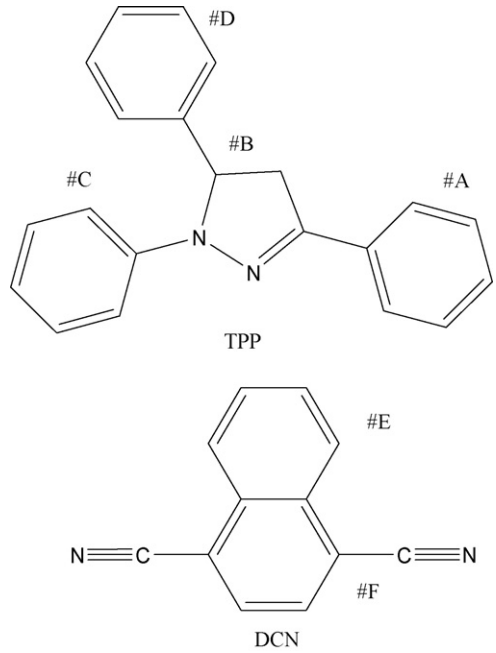

Fig. 1. Chemical structure of the TPP and DCN complex.

and μ_{11} is the static dipole moment and μ_{01} is the transition dipole, respectively).

To visualize all molecular orbitals involved in transitions to the excited state, several elaborate theoretical approaches have been developed. One is the 2D site representation of transition density matrix [22–24], which provides visual information of electron–hole coherence and the excitation delocalization region of conjugated molecule upon excitation. Another one is the 3D cube representation of transition density (TD) and charge difference density (CDD) [25–28], which has been employed to study CT process of several conjugated polymers.

In this paper, we perform quantum chemical calculation as well as two-dimensional (2D) site and three-dimensional (3D) cube studies on the mixed coaggregates with electron-rich 1,3,5-triphenyl-2-pyrazoline (TPP) and electron-deficient 1,4-dicyanonaphthalene (DCN) (see Fig. 1) [29], to provide a deeper insight into excited state properties and to reveal CT mechanism of the system. The article is organized as follows: Firstly, the nature of electronic state in absorption for TPP and DCN is examined in detail, respectively. Subsequently, we will describe a detailed analysis of the excited state properties and CT process for TPP and DCN complex with 2D site and 3D cube representations. The excited region and change of charge density, as the result of electronic orbital transition, can be employed as the useful evidence to explore the CT process for TPP and DCN complex in the vertical absorption.

2. Methods

Geometry optimizations of TPP, DCN and the TPP–DCN complex in the ground state were performed using density functional theory (DFT) [30], with Becke's three-parameter hybrid exchange functional (B3LYP) [31] at the 6-31G (d) basis set level. Vibration frequency calculation was conducted to confirm the stability of the optimized geometry. Electronic transition energies and oscillator strengths were calculated at these geometries using time-dependent density functional theory (TD-DFT) [32] at the same functional and basis set. All the calculations were done with Gaussian 03 suite [33].

To understand the nature of the excited states, we have used the result of the TD-DFT calculation to obtain two-dimensional (2D) electron–hole two-particle wave functions [22–24], which leads to a two-dimensional grid that – for each of the axes – runs over all the carbon sites:

$$\left|\Psi(x,y)\right|^2 = \sum_{q\in x}\sum_{r\in y}\left|\psi(q,r)\right|^2 \tag{3}$$

For each data point (x,y) in two-dimensional grid, $|\psi(x,y)|^2$ gives the probability of finding one charged particle of the "exciton" in atomic orbital q on site x and the second in atomic orbital r on site y. These two-dimensional maps provide insight into the size of excitation delocalization along the diagonal part [22], the size of the exciton along the off diagonal part [23], and the amount of excited-state localization on the different parts of the model compounds [24].

In the 3D cube representation, the transition density (TD) from the ground state (S_0) to excited state (S_u) is described as [25–27]:

$$\rho_{u0}(\vec{r}) = \sum_{\substack{\alpha\in unoc\\ i\in occ}} C_{uai}\varphi_a(\vec{r})\varphi_i(\vec{r}) \tag{4}$$

where C_{uai} represents the uth eigenvector of the configuration-interaction (CI) Hamiltonian based on the single excitations from the occupied Hartree–Fock molecular orbital $\varphi_i(\vec{r})$ to the unoccupied one $\varphi_a(\vec{r})$. Transition density (TD) determines the dipole transition moment (or transition dipole) [26,27], indicating the strength and the orientation for the interaction:

$$\vec{\mu}_{u0} = \int \vec{r}\rho_{\mu 0}(\vec{r})d^3\vec{r} \tag{5}$$

The charge difference density (CDD) shows the orientation and results of the charge and energy transfer [24,26–28]:

$$\Delta\rho_{\mu\mu}(\vec{r}) = \sum_{\substack{a\in unocc\\ i,j\in occ}} C_{\mu aj}C_{\mu ai}\varphi_j(\vec{r})\varphi_i(\vec{r}) - \sum_{\substack{a,b\in unocc\\ i\in occ}} C_{\mu aj}C_{\mu ai}\varphi_b(\vec{r})\varphi_a(\vec{r}) \tag{6}$$

The first and the second terms in Eq. (6) stand for hole and electron, respectively.

3. Results and discussion

3.1. Excited state properties of TPP

The calculated transition energies and oscillator strengths for TPP monomer are listed in Table 1. Within the considered energy range, there are three strong electronic transitions of sizable intensity ($f > 0.1$), corresponding to S_1, S_7 and S_9 excited states, respectively. The TD-DFT calculated transition energy ($S_0 \rightarrow S_1$) is found at 358.03 nm (Exp. 365 nm). This slight discrepancy between experiment and simulation can be contributed to the fact that solvent effect is not considered in the calculation. According to CI main coefficients, the S_1 state is composed of the HOMO → LUMO transition. As the result of molecular orbital transition, 3D cube representation of transition density and charge difference density reveals the nature of that characteristic electronic transition, as discussed below.

Photoinduced electron transfer results in charge redistribution, and thus molecules undergo obvious changes in dipole moment. To visualize the contribution of the molecular orbital to electronic transition, the 3D cube representation of transition density is investigated, which reveals the orientation and strength of the transition dipole moments. From transition density of S_1 state (see Fig. 2),

Table 1
Calculated transition energies (eV, nm) and oscillator strengths (*f*) for TPP monomer.

	Transition energy, eV (nm)	Oscillator strength, *f*	CI coefficients for electronic transition	λ_{abs}^{exp} (nm)
S_1	3.4630 (358.03)	0.5528	0.6457 (H → L)	365
S_2	3.9989 (310.05)	0.0103		
S_3	4.0672 (304.84)	0.0039		
S_4	4.3158 (287.28)	0.0159		
S_5	4.5158 (274.56)	0.0146		
S_6	4.9183 (252.09)	0.0047		
S_7	4.9769 (249.12)	0.2384	0.51007 (H−2 → L); 0.28266 (H−1 → L); −0.32175 (H → L+5)	
S_8	5.0821 (243.96)	0.0043		
S_9	5.1070 (242.78)	0.1236	0.54328 (H−4 → L); 0.18155 (H−2 → L+3); −0.14465 (H → L+3); 0.28574 (H → L+5)	

Experimental absorption wavelength of TPP in water taken from Ref. [29].

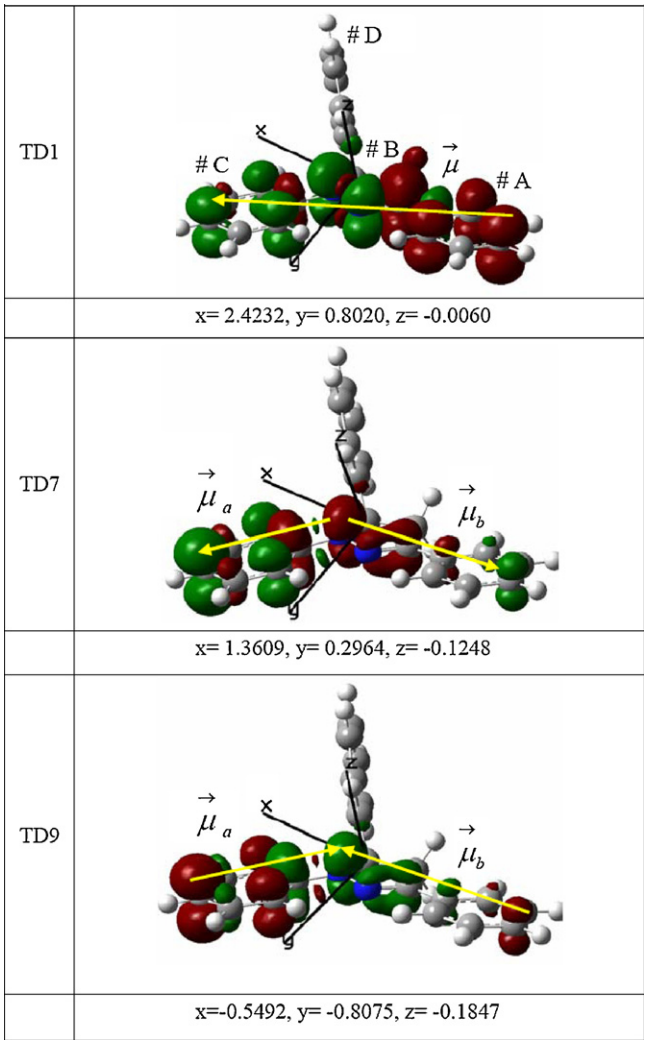

Fig. 2. Transition densities of the three excited states ($f > 0.1$) for TPP monomer. The green and red colors stand for the hole and electron, respectively, and the isovalue is 1×10^{-4} a.u. The transition moments (a.u.) were listed below, and Cartesian coordinates were given at the same time. (For interpretation of the references to color in this figure legend, the reader is referred to the web version of the article.)

one find that red electrons mainly reside in #A and green holes are mainly localized in #C, and so the orientation of transition dipole moment is from #A to #C (from red electron to green hole). It is worthy noting that the #D contributes little to the transition density of the S_1.

For the S_7 and S_9 states, the main contribution to transition density also originate from #A, #B and #C units, but they display different distribution of transition density closed to the absorption strength. From transition density of S_7 (see Fig. 2), there are two subtransition dipoles ($\vec{u}_a$ and $\vec{u}_b$), with the "tail to tail" character, since red electrons are mainly localized on #B and green holes are localized on two sides. The opposite orientation of two subtransition dipole moments weaken the total transition dipole moment ($\vec{u}_{tol} = \vec{u}_a + \vec{u}_b$) to a large extent, and thus the total transition dipole moment of S_7 state is smaller than that of S_1 state. For the S_9 state, it also has the two subtransition dipole moments with opposite orientation, exhibiting the "head to head" character. According to the relationship between transition dipole moment and oscillator strength [27], $|\mu|^2 \propto f/E$ (where μ, f and E stand for transition dipole moment, oscillator strength and excitation energy, respectively), the S_7 and S_9 oscillator strengths become smaller than that of S_1 state. It is the reason why S_1 state has a strong absorption peak in the UV–vis spectra.

The 3D cube representation of charge difference density, as a visual evidence of the orientation and result of charge transfer, enable us to follow the change of the static charge distribution upon excitation. It is clearly shown in Fig. 3 that for S_1 state the hole is mainly localized on #C unit, and the electrons are mainly localized on #A unit, so it is intramolecular charge transfer (ICT) excited state, and the charge transfer from #C unit to #A unit. From charge difference density of S_9 state, this state is also ICT state, but it is different from the ICT of S_1 state, for S_9 state, the holes are mainly localized in #D unit (the excitation of phenyl ring [3]), i.e. the ICT is from #D unit to the other units.

3.2. Excited state properties of DCN

The transition energies and oscillator strengths of DCN monomer are listed in Table 2. From Table 2, the S_4 state is of the largest oscillator strength *f*; while for S_1 and S_3, they have closed oscillator strength *f* (0.1360 and 0.1552, respectively). The three absorption peaks ($f > 0.1$) of DCN are related to the three prominent transitions: S_1 located at 334.69 nm (Exp. 335 nm), S_3 at 249.39 nm

Table 2
Calculated transition energies (eV, nm) and oscillator strengths (*f*) for DCN monomer.

	Transition energies, eV (nm)	Oscillator strength, *f*	CI coefficients for electronic transition	λ_{abs}^{exp} (nm)
S_1	3.7045 (334.69)	0.1360	0.16531 (H−2 → L); 0.10841 (H−1 → L+1); 0.62983 (H → L)	335
S_2	4.1993 (295.25)	0.0300		
S_3	4.9714 (249.39)	0.1552	0.61891 (H−2 → L); −0.10519 (H → L); 0.23720 (H → L+2)	
S_4	5.4465 (227.64)	0.4938	−0.16951 (H−3 → L); 0.28733 (H−1 → L); 0.27554 (H−1 → L+2); 0.47907 (H → L+1)	

Experimental absorption wavelength of DCN in water taken from Ref. [29].]

Table 3
Calculated transition energies (eV, nm) and oscillator strengths (*f*) for TPP–DCN.

	Transition energy, eV(nm)	Oscillator strength, *f*	CI coefficients for electronic transition	Abs (Os)[a]
S_1	1.8206 (681.00)	0.0017	0.70621 (H → L)	627 (0.0086)
S_2	3.3433 (370.85)	0.0594		
S_3	3.4072 (363.88)	0.0014		
S_4	3.4423 (360.18)	0.2940	0.13342 (H−3 → L); 0.47470 (H → L+1); −0.43079 (H → L+2)	355 (0.2609)

[a] The data of TPP–DCN complex from Ref. [29], where Abs and Os represent absorption peak and oscillator strength, respectively.

and S_4 at 227.64 nm. Though S_1 and S_3 states have closed oscillator strength, they have different characteristic features. As shown in Fig. 4, the transition density of S_1 state alternates in sign on the #E and #F units, which should be represented by a series of small transition dipoles—one per monomeric unit [28]. The orientation of total transition dipole moments for S_1 state (see Fig. 4) is from the right to left side of molecule (opposite to the molecular *x*-axis). As for S_3 state, the transition density is mainly concentrated on #E unit, and the orientation of transition dipole moments is opposite to that of S_1 state. Calculated transition dipole moments are listed below the corresponding figure of the transition density, and Cartesian coordinates are given at the same time. For S_4 state, electron and hole are localized on #E and #F units, where the two subtransition dipole moments have the same orientations. The ori-

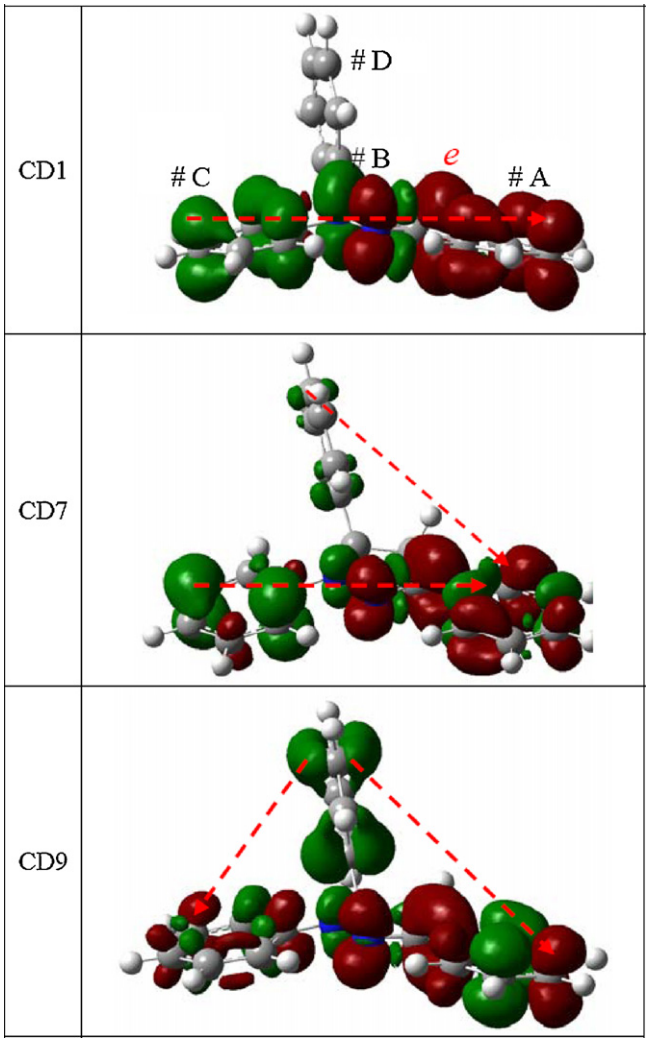

Fig. 3. Charge difference densities of the three excited states for TPP monomer. The green and red colors stand for the hole and electron, respectively, and the isovalue is 1×10^{-4} a.u. (For interpretation of the references to color in this figure legend, the reader is referred to the web version of the article.)

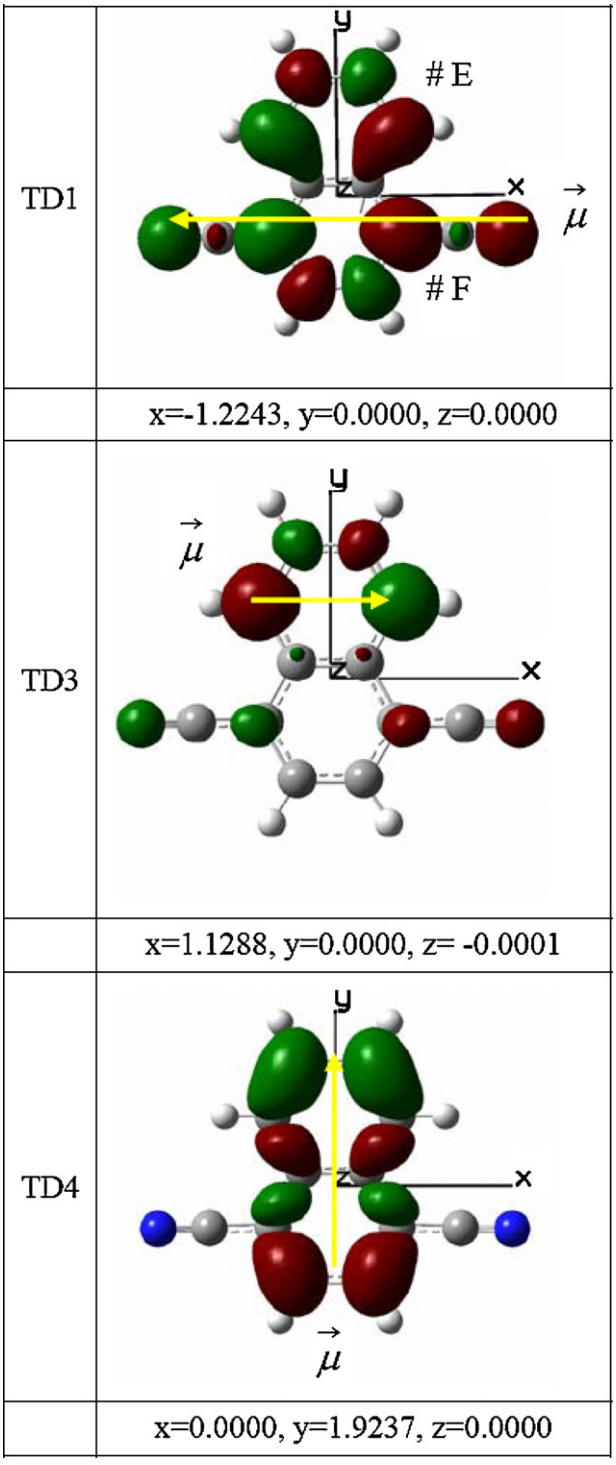

Fig. 4. Transition densities of the three excited states ($f > 0.1$) for DCN monomer. The green and red colors stand for the hole and electron, respectively, and the isovalue is 1×10^{-4} a.u. The transition moments (a.u.) were listed below, and Cartesian coordinates were given at the same time. (For interpretation of the references to color in this figure legend, the reader is referred to the web version of the article.)

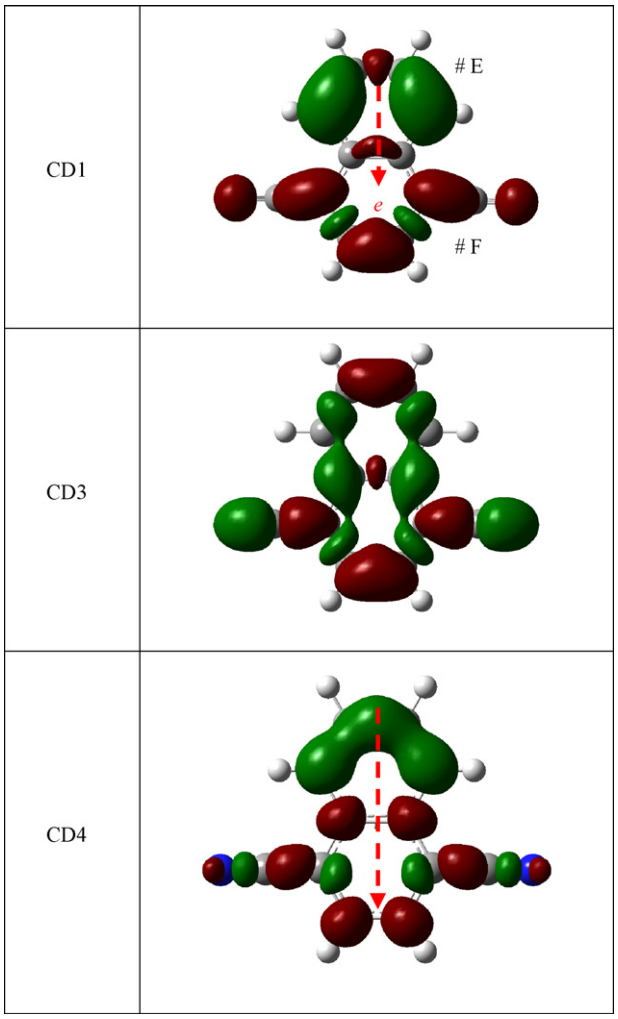

Fig. 5. Charge difference densities of the three excited states for DCN monomer. The green and red colors stand for the hole and electron, respectively, and the isovalue is 1×10^{-4} a.u. (For interpretation of the references to color in this figure legend, the reader is referred to the web version of the article.)

entation of total transition dipole is from #F to #E (alone molecular *y*-axis).

From the charge difference density of S_1 state (see Fig. 5), this state is ICT excited state, and charge transfer occurs from #E to #F. For S_3 state, electron–hole pairs distribute over double and single bonds, and ICT is not found between the two units, and thus this sate is characterized as π–π^* transition of exchange of the double and single bonds. While for S_4 state, more electrons are excited to #F and more holes are left on #E, leading to the strong transition dipole moment along *y*-axis (see transition density, in Fig. 4).

3.3. Excited state properties of TPP–DCN

The calculated transition energies and oscillator strengths of TPP and DCN complex are listed in Table 3, and calculated value is consistent with previous report [29]. From Table 3, calculated result shows that the main absorption band of TPP–DCN complex is assigned to the transition from the ground state S_0 to the S_4 state with a larger oscillator strength $f = 0.2940$ (0.2609 [29]); while for S_1 state, it is a "dark" state with a low oscillator strength. For S_4 state, according to CI main coefficients of the orbital transition (listed in Table 3), the main contribution comes from the orbital transition from HOMO to LUMO+1. It should be noted that for the orbital transition of TPP and DCN complex from HOMOs to LUMOs, the HOMO−3 and LUMO+2 have to be also considered, since the S_4 state is mainly composed of HOMO−3 → LUMO, HOMO → LUMO+1, and HOMO → LUMO+2 orbitals transition, and CI coefficients are 0.13342 (HOMO−3 → LUMO), 0.47470 (HOMO → LUMO+1), and −0.43079 (HOMO → LUMO+2), respectively. In this contribution, we calculated two-dimensional electron–hole two-particle wave functions, which considered all contribution of molecular orbitals to excitation, to establish a direct real-space connection between the optical response and motions of charge in the molecule upon optical excition.

The incident light moves an electron from an occupied orbital to an unoccupied orbital, creating an electron–hole pair or an exciton. From the 2D site representation of transition densities matrix (see Fig. 6(b)), electron–hole coherence sizes remain localized in the #A, B, C of TPP and the whole DCN (off-diagonal elements [23]). This means that charge transfer occurs between TPP and DCN monomers. Along the diagonal elements [22], a strong delocalized size distribute over #A unit of TPP monomer during excitation, where the extra electrons originate from some segments of electron-rich TPP monomer through intramolecular CT process. Charge different density supports the above analysis and visualizes the orientation of CT. From charge different density (see Fig. 7), holes are left on #C unit of TPP, and electrons move to #A of TPP and DCN, respectively. So, photoinduced intermolecular CT occurs from TPP to DCN, and intramolecular CT occurs on TPP monomer (the orientation of CT is from #C to #A). Direct visual evidence revealed that for the mixed coaggregates of TPP and DCN, the strong absorption band originates from a mixed inter- and intra-molecular CT process. It is a very interesting phenomenon occurring in mixed coaggregate systems which consist of electron-rich TPP as a donor and electron-deficient DCN as an acceptor.

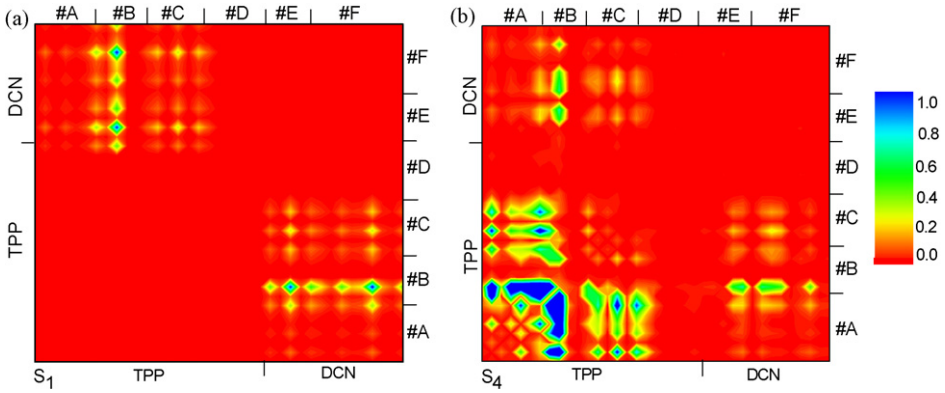

Fig. 6. The 2D site representation of transition densities matrix for TPP–DCN complex, where the label of units can be seen from Fig. 1.

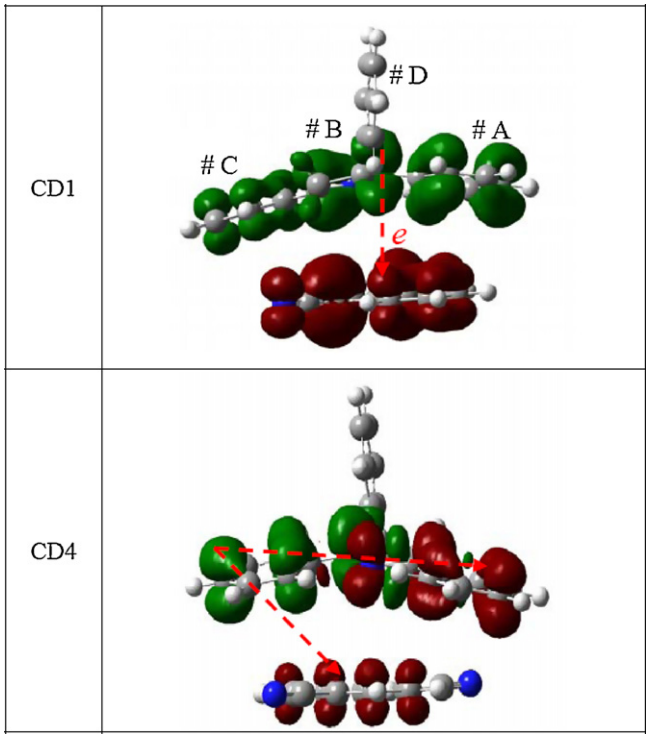

Fig. 7. Charge difference densities of two excited states for TPP–DCN complex. The green and red colors stand for the hole and electron, respectively, and the isovalue is 1×10^{-4} a.u. (For interpretation of the references to color in this figure legend, the reader is referred to the web version of the article.)

For S_1 state, it is a "dark" state with a low oscillator strength, and excited state properties are further investigated with the 2D site and 3D cube representations. As shown in Fig. 6(a), electron–hole coherence sizes is over the #A, #B and #C of TPP and the DCN. In this region, strong rearrangement of the electron density occurs by the excitation process. From the charge different density (see Fig. 7), green holes reside in TPP monomer and red electrons move to DCN monomer, and the CT occurs from TPP to DCN. So, the "dark" state belongs to intermolecular CT excited state.

4. Conclusion

The charge transfer and excited state properties for mixed coaggregates of TPP and DCN were studied using TD-DFT as well as 2D site and 3D cube representations. 2D site representation of transition density matrix shows electron–hole coherence and the excitation delocalization during excitation. The 3D cube representation of transition density visualizes the orientation and strength of the transition dipole moment, and the 3D cube representation of charge difference density gives the orientation and result of the charge transfer. Direct visual evidence indicates that (1) the intermolecular CT occurs between TPP donor and DCN acceptor and (2) the intramolecuar CT phenomenon is found to take place in TPP monomer. The #C unit of TPP monomer not only serves as the electronic donor in the intramolecular CT, but also in the intremolecular CT process. The CT mechanism for the mixed coaggregates of TPP and DCN is found to be the mixture of the intermolecular and intramolecular CT in the absorption process. The conclusion drawn by 2D and 3D real-space analysis is a valuable clue for the future design of multifunctional architectures and nanostructured materials for artificial photoelectronic devices.

Acknowledgements

This work was supported by the National Natural Science Foundation of China (Grant Nos. 10604012, 20703064 and 10874234) and SRF for ROCS, SEM (2006).

References

[1] J.L. Bredas, D. Beljonne, V. Coropceanu, J. Cornil, Chem. Rev. 104 (2004) 4971–5003.
[2] N. Mataga, H. Chosrowjan, S. Taniguchi, J. Photochem. Photobiol. C: Photochem. Rev. 6 (2005) 37–79.
[3] H.B. Fu, J.N. Yao, J. Am. Chem. Soc. 123 (2001) 1434–1439.
[4] (a) G.J. Zhao, R.K. Chen, M.T. Sun, J.Y. Liu, G.Y. Li, Y.L. Gao, K.L. Han, X.C. Yang, L. Sun, Chem. Eur. J. 14 (2008) 6935–6947;
(b) M.T. Sun, H.X. Xu, ChemPhysChem 10 (2009) 392–395.
[5] D.W. Cho, M. Fujitsuka, U.C. Yoon, T. Majima, Phys. Chem. Chem. Phys. 10 (2008) 4393–4399.
[6] S. Kim, J.K. Lee, S.O. Kang, J. Ko, J.H. Yum, S. Fantacci, F. De Angelis, D. Di Censo, M.K. Nazeeruddin, M. Gratzel, J. Am. Chem. Soc. 128 (2006) 16701–16707.
[7] Y. Kashiwagi, K. Ohkubo, J.A. McDonald, I.M. Blake, M.J. Crossley, Y. Araki, O. Ito, H. Imahori, S. Fukuzumi, Org. Lett. 5 (2003) 2719–2721.
[8] A. Amadei, M. D'Abramo, A. Di Nola, A. Arcadi, G. Cerichelli, M. Aschi, Chem. Phys. Lett. 434 (2007) 194–199.
[9] M.T. Sun, L.W. Liu, Y. Ding, H.X. Xu, J. Chem. Phys. 127 (2007) 084706–084708.
[10] R.S. Lokey, B.L. Iverson, Nature 375 (1995) 303–305.
[11] A.F.M. Kilbinger, R.H. Grubbs, Angew. Chem. Int. Ed. 41 (2002) 1563–1566.
[12] L.Y. Park, D.G. Hamilton, E.A. McGehee, K.A. McMenimen, J. Am. Chem. Soc. 125 (2003) 10586–10590.
[13] Z.H. Wang, F. Dotz, V. Enkelmann, K. Mullen, Angew. Chem. Int. Ed. 44 (2005) 1247–1250.
[14] E.H.A. Beckers, P. Jonkheijm, A. Schenning, S.C.J. Meskers, R.A.J. Janssen, ChemPhysChem 6 (2005) 2029–2031.
[15] M. Fardy, P.D. Yang, Nature 451 (2008) 408–409.
[16] D.W. Cho, M. Fujitsuka, U.C. Yoon, T. Majima, J. Photochem. Photobiol. A: Chem. 190 (2007) 101–109.
[17] M. Pope, C.E. Swenberg, Electronic Processes in Organic Crystals, Oxford University Press, New York, 1999.
[18] T. Del Cano, J.A. de Saja, R.F. Aroca, Chem. Phys. Lett. 377 (2003) 347–353.
[19] P.H. Kwan, T.M. Swager, J. Am. Chem. Soc. 127 (2005) 5902–5909.
[20] R.S. Mulliken, W.B. Person, Molecular Complexes, Wiley, NewYork, 1969.
[21] G. DeBoer, A. Preszler Prince, M.A. Young, J. Chem. Phys. 115 (2001) 3112–3120.
[22] S. Mukamel, S. Tretiak, T. Wagersreiter, V. Chernyak, Science 277 (1997) 781–787.
[23] S. Tretiak, A. Saxena, R.L. Martin, A.R. Bishop, Phys. Rev. Lett. 89 (2002) 0974021–0974024.
[24] M.T. Sun, Y. Ding, H.X. Xu, J. Phys. Chem. B 111 (2007) 13266–13270.
[25] B.P. Krueger, G.D. Scholes, G.R. Fleming, J. Phys. Chem. B 102 (1998) 5378–5386.
[26] K.G. Jespersen, W.J.D. Beenken, Y. Zaushitsyn, A. Yartsev, M. Andersson, T. Pullerits, V. Sundstrom, J. Chem. Phys. 121 (2004) 12613–12617.
[27] M.T. Sun, P. Kjellberg, W.J.D. Beenken, T. Pullerits, Chem. Phys. 327 (2006) 474–484.
[28] M.T. Sun, J. Chem. Phys. 124 (2006) 54903–54906.
[29] F.G. Shen, A.D. Peng, Y. Chen, Y. Dong, Z.W. Jiang, Y.B. Wang, H.B. Fu, J.N. Yao, J. Phys. Chem. A 112 (2008) 2206–2210.
[30] M.R. Dreizler, E.K.U. Gross, Density Functional Theory, Springer Verlag, Heidelberg, Germany, 1990.
[31] C. Lee, W. Yang, R.G. Parr, Phys. Rev. B 37 (1998) 785–789.
[32] E.K.U. Gross, W. Kohn, Phys. Rev. Lett. 55 (1985) 2850–2852.
[33] M.J.T. Frisch, et al., Computed Code Gaussian 03, Revision B.05, Gaussian, Inc., Pittsburgh, PA, 2003.